

Hybrid Arrays: How Many RF Chains Are Required to Prevent Beam Squint?

Heedong Do, *Member, IEEE*, Namyoon Lee, *Senior Member, IEEE*, Robert W. Heath Jr., *Fellow, IEEE*, Angel Lozano, *Fellow, IEEE*

Abstract—With increasing frequencies, bandwidths, and array apertures, the phenomenon of beam squint arises as a serious impairment to beamforming. Fully digital arrays with true time delay per antenna element are a potential solution, but they require downconversion at each element. This paper shows that hybrid arrays can perform essentially as well as digital arrays once the number of radio-frequency chains exceeds a certain threshold that is far below the number of elements. The result is robust, holding also for suboptimum but highly appealing beamspace architectures.

Index Terms—Wideband communication, beam squint, spatial wideband effect, hybrid beamforming, mmWave frequencies, terahertz frequencies

I. INTRODUCTION

In the quest for fresh spectrum, there is much interest in millimeter wave (mmWave) and sub-terahertz bands [1]. Enormous amounts of bandwidth can be put into service at these frequencies, contingent on high-gain antennas to overcome the rising noise floor [2]–[5]. For the sake of reconfigurability, antenna arrays composed of multiple low-gain elements are preferred over a single high-gain antenna. Given that hundreds of such elements become necessary, fully digital arrays with one radio-frequency (RF) chain per element are unaffordable in terms of power consumption and cost [6]–[8]. Fully analog designs with one RF chain per array must be resorted to, with the drawback that, while the channel is frequency-dependent, analog phase shifters are frequency-independent. This results in diminished antenna gains at frequencies away from the central one, at which the array is optimized, in a phenomenon termed *beam squint* [9, Ch. 1.2].

While this phenomenon can in principle be corrected with true-time-delay (TTD) beamforming [10]–[14], the required delays for array sizes of interest are not available at mmWave frequencies when implemented at RF (see [15, Table I] and [16, Table I]) and, in any event, a large chip area would be consumed. Digital true-time-delay beamforming does offer a

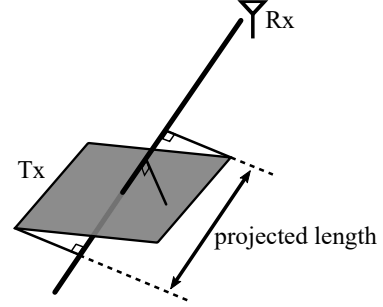


Fig. 1. Projection of a planar array onto the direction of beamforming, yielding a line segment.

much broader range of delays [16, Table II], but again it necessitates of downconversion to baseband at each antenna element. Hybrid arrays lie between the two extremes, fully analog and fully digital, and offer potentially the best of both worlds in terms of performance and cost. The analysis of beam squint in hybrid arrays is therefore of importance, yet, in contrast with analog arrays, for which the beam-squint loss has been quantified with theoretical guarantees [9], only algorithmic approaches are available for hybrid arrays [17]–[21]. In the wake of recent contributions [22]–[26], this paper tackles the following research questions:

- 1) What is the beam-squint loss in beamforming gain when using hybrid arrays in lieu of fully digital ones?
- 2) Is there a number of RF chains beyond which this loss vanishes and, if so, what is that number?

Remarkably, the latter question is answered in the affirmative. The minimum number of RF chains required to do away with the beam-squint loss emerges in a surprisingly compact closed form. For a linear array, this minimum number is simply

$$\frac{\text{bandwidth}}{\text{carrier frequency}} \cdot \frac{\text{projected length}}{\text{wavelength}} \quad (1)$$

where “projected length” refers to the array’s projection onto the direction of beamforming. The scope extends readily to planar arrays, only with that projected length generalized to being the length of the longest segment that the array projects onto the direction of beamforming (see Fig. 1).

As the product of carrier frequency and wavelength equals the speed of light, c , the above can equivalently be expressed via the raw bandwidth and raw projected length, namely

$$\frac{1}{c} \cdot \text{bandwidth} \cdot \text{projected length}. \quad (2)$$

H. Do and N. Lee are with the School of Electrical Engineering, Korea University, 02841 Seoul, South Korea (e-mail: {doheedong, namyoon}@korea.ac.kr). Their work is supported in part by the Institute of Information & Communications Technology Planning & Evaluation (IITP) under Grant 2021-0-00161 and in part by the National Research Foundation of Korea (NRF) under Grant 2023-00208552, both funded by the Korea Government (MSIT). A. Lozano is with Univ. Pompeu Fabra, 08018 Barcelona (e-mail: angel.lozano@upf.edu). His work is supported by the Maria de Maeztu Units of Excellence Programme (MDM-2021-001195-M), by the Fractus-UPF Chair on Tech Transfer and 6G, and by ICREA. Robert W. Heath Jr. is with the Department of Electrical and Computer Engineering, North Carolina State University, 890 Oval Dr., Raleigh, NC, 27606, USA (e-mail: rwheathjr@ncsu.edu).

In rather broad generality, this product of the bandwidth and the projected array length dictates the severity of the beam squint, and it directly gives the minimum number of RF chains required for squint-free beamforming with a hybrid array. Growing bandwidths, expanding array apertures, and beamforming directions deviating from broadside, all exacerbate the squint and call for a larger number of RF chains in (2), yet a hybrid array equipped with that many chains can always beamform without squint. This behavior is asymptotic, in the sense that the squint vanishes as the product grows large, yet it very faithfully describes the behavior for the values of interest.

For an array intending to beamform in any direction, the projected length in (2) must be set to its highest value, which is the actual length (for a linear array) or the diagonal length (for a planar array).

The findings summarized above and expounded in the sequel are robust, holding not only for optimum beamforming, but further for suboptimal beamspace architectures consisting of a bank of beams with a regular disposition [27]. The existence of a number of RF chains beyond which the squint vanishes holds even if the connectivity within the hybrid array is restricted, in the so-called hybridly-connected structure where the array is partitioned into subarrays and each subarray is connected only to a subset of RF chains. An interesting tradeoff then arises in that the number of analog phase shifters shrinks at the expense of an increased number of RF chains. Reducing both the number of analog phase shifters and RF chains leads to some residual squint being fundamentally inevitable, an aspect that we quantify for the case of a single RF chain per subarray.

The paper is organized as follows. Sec. II introduces the system model and Sec. III describes the phenomenon of beam squint. A simple criterion for squint-free operation is set forth in Sec. IV. Then, the minimum number of RF chains required for squint-free operation is quantified for linear and planar arrays in Secs. V and VI, respectively. The foregoing analyses are numerically validated in Sec. VII. In Sec. VIII, the results are extended to simpler architectures with restricted connectivity, and also to a multiantenna receiver. Finally, the paper concludes in Sec. IX.

II. SYSTEM MODEL

A. Array Model

Consider a UPA-equipped transmitter and a single-antenna receiver. The UPA has dimensionality $N_x \times N_y$ and aperture $L_x \times L_y$, whereby the element spacings along the respective dimensions are $d_x = \frac{L_x}{N_x}$ and $d_y = \frac{L_y}{N_y}$.

The coordinate system is such that the n th transmit element ($n \in \{0, \dots, N-1\}$ with $N = N_x N_y$) is at

$$\begin{bmatrix} x_n & y_n & 0 \end{bmatrix}^\top = \begin{bmatrix} d_x(n_x - \frac{N_x-1}{2}) & d_y(n_y - \frac{N_y-1}{2}) & 0 \end{bmatrix}^\top$$

where $n_x \in \{0, \dots, N_x-1\}$ and $n_y \in \{0, \dots, N_y-1\}$ are the quotient and remainder of n/N_y . The receiver is located at $D [\sin \phi \cos \theta \quad \sin \phi \sin \theta \quad \cos \phi]^\top$ where D is the communication range, ϕ is the zenith angle, and θ is the

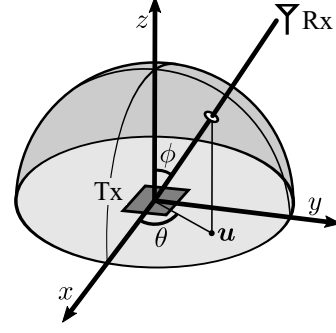


Fig. 2. Considered geometry, including \mathbf{u} and a unit hemisphere as reference.

azimuth angle (see Fig. 2). For convenience, let us henceforth define

$$\mathbf{r}_n = [x_n \quad y_n]^\top \quad \mathbf{u} = [u_x \quad u_y]^\top \quad (3)$$

where $u_x = \sin \phi \cos \theta$ and $u_y = \sin \phi \sin \theta$. Note that \mathbf{u} , also depicted in Fig. 2, corresponds to the uv -coordinates, handy for many applications including array processing [9]. It is a convenient two-dimensional projection of the unit-vector pointing to the receiver; the higher its magnitude, the further from broadside, with $\|\mathbf{u}\| = 0$ and $\|\mathbf{u}\| = 1$ respectively denoting the exact broadside and endfire directions.

The consideration of UPAs does not exclude uniform linear arrays (ULAs), as the latter are a special case of the former. Our convention for linear arrays is to set $N_y = 1$.

B. Channel Model

We posit a line-of-sight (LOS) connection. Denoting the carrier frequency by f_c , and the frequency relative to it by $f \in [-\frac{W}{2}, \frac{W}{2}]$ with W the bandwidth, the n th entry of the normalized channel vector \mathbf{a}^* at $f_c + f$ is

$$[\mathbf{a}^*(f)]_n = \exp\left(j2\pi \frac{f_c + f}{c} \mathbf{u}^\top \mathbf{r}_n\right). \quad (4)$$

Such channel vector can be expressed as [9, Eq. 1.59]

$$\mathbf{a}^*(f) = \mathbf{a}_x^*(f) \otimes \mathbf{a}_y^*(f) \quad (5)$$

where $\mathbf{a}_x(f) \in \mathbb{C}^{N_x}$ and $\mathbf{a}_y(f) \in \mathbb{C}^{N_y}$ are vectors with entries

$$[\mathbf{a}_x^*(f)]_n = \exp\left(j2\pi \frac{f_c + f}{c} u_x x_n\right) \quad (6)$$

$$[\mathbf{a}_y^*(f)]_n = \exp\left(j2\pi \frac{f_c + f}{c} u_y y_n\right). \quad (7)$$

The amplitude factor omitted by the normalization can be directly incorporated into the signal-to-noise ratio, giving¹

$$\text{SNR} = \frac{\lambda^2 G_t G_r P_t}{(4\pi D)^2 W N_0} \quad (8)$$

where G_t and G_r are the transmit and receive element gains, P_t is the total radiated power, and N_0 is the noise spectral density.

¹Large-scale effects such as atmospheric attenuation [28], which is not negligible for long-range transmissions, can be easily incorporated.

C. Signal Model

A hybrid array is considered, with the number of RF chains being N_{RF} . Denoting the analog and digital beamforming stages by $\mathbf{W}_a \in \mathbb{C}^{N \times N_{\text{RF}}}$ and $\mathbf{w}_d(f) \in \mathbb{C}^{N_{\text{RF}}}$, respectively, the relation between the transmit signal $s(f)$ and the receive signal $y(f)$ is given by

$$y(f) = \mathbf{a}^*(f) \mathbf{W}_a \mathbf{w}_d(f) s(f) + v(f) \quad (9)$$

where $v(f)$ is a white Gaussian noise process with unit power spectral density. A single signal stream is transmitted, as the channel is of rank one.

Letting $s(f)$ have unit power, the power constraint becomes

$$\frac{1}{W} \int_{-\frac{W}{2}}^{\frac{W}{2}} \|\mathbf{W}_a \mathbf{w}_d(f)\|^2 df = \text{SNR}. \quad (10)$$

Introducing

$$p(f) = \|\mathbf{W}_a \mathbf{w}_d(f)\|^2 \quad (11)$$

$$g(f) = \frac{|\mathbf{a}^*(f) \mathbf{W}_a \mathbf{w}_d(f)|^2}{\|\mathbf{W}_a \mathbf{w}_d(f)\|^2}, \quad (12)$$

we can succinctly rewrite the signal model as

$$y(f) = \sqrt{g(f)p(f)} s(f) + v(f) \quad (13)$$

with the streamlined power constraint

$$\frac{1}{W} \int_{-\frac{W}{2}}^{\frac{W}{2}} p(f) df = \text{SNR}. \quad (14)$$

Respectively, $g(f)$ and $p(f)$ can be interpreted as the beamforming gain and transmit power at frequency f .

For a given analog beamformer, we can optimize the digital beamformer. To do so, we introduce the auxiliary quantity [29, Lemma 5]

$$\tilde{\mathbf{w}}_d(f) \equiv (\mathbf{W}_a^* \mathbf{W}_a)^{\frac{1}{2}} \mathbf{w}_d(f), \quad (15)$$

which is a natural choice from

$$p(f) = \mathbf{w}_d^*(f) (\mathbf{W}_a^* \mathbf{W}_a) \mathbf{w}_d(f) \quad (16)$$

$$= \|\tilde{\mathbf{w}}_d(f)\|^2. \quad (17)$$

Plugging (15) into (12), we obtain

$$g(f) = \frac{\|\mathbf{a}^*(f) \mathbf{W}_a (\mathbf{W}_a^* \mathbf{W}_a)^{-\frac{1}{2}} \tilde{\mathbf{w}}_d(f)\|^2}{\|\tilde{\mathbf{w}}_d(f)\|^2} \quad (18)$$

$$\leq \|(\mathbf{W}_a^* \mathbf{W}_a)^{-\frac{1}{2}} \mathbf{W}_a^* \mathbf{a}(f)\|^2 \quad (19)$$

where the upper bound follows from the Cauchy-Schwarz inequality. For any $p(f)$, such bound can be attained by

$$\tilde{\mathbf{w}}_d(f) = \sqrt{p(f)} \frac{(\mathbf{W}_a^* \mathbf{W}_a)^{-\frac{1}{2}} \mathbf{W}_a^* \mathbf{a}(f)}{\|(\mathbf{W}_a^* \mathbf{W}_a)^{-\frac{1}{2}} \mathbf{W}_a^* \mathbf{a}(f)\|}. \quad (20)$$

III. BEAM SQUINT

The beam squint effect is evidenced by observing the beamforming gain behavior on the space-frequency plane. To make the dependence on both space and frequency explicit, in this section the notation $\mathbf{a}(\mathbf{u}, f)$ and $g(\mathbf{u}, f)$ is used in lieu of $\mathbf{a}(f)$ and $g(f)$ when appropriate.

With a unit-norm analog combiner \mathbf{w}_a and no digital combiner, (12) reduces to

$$g(\mathbf{u}, f) = |\mathbf{w}_a^* \mathbf{a}(\mathbf{u}, f)|^2, \quad (21)$$

which is often termed *beam pattern* in terms of its dependence on \mathbf{u} [9]. From (4),

$$\mathbf{a}^*(\mathbf{u}, f) = \mathbf{a}^*((1 + f/f_c)\mathbf{u}, 0), \quad (22)$$

which gives

$$g(\mathbf{u}, f) = g((1 + f/f_c)\mathbf{u}, 0). \quad (23)$$

This implies that the beam pattern at $f_c + f$ is a scaled version of that at f_c . Accordingly, the peak of the formed beam changes its direction with the frequency, which is why the phenomenon is termed beam squint; only perfectly broadside beams are immune. This argument is valid for any array geometry and beamformer, therefore it is essentially a generalization of [26, Lemma 2].

As a guideline for when the squint becomes significant, the notion of 3-dB loss in beamforming gain is often used [9, Ch. 1.2]. For ease of exposition, consider an N -element ULA on the x -axis and maximum ratio transmission (MRT), whereby $\mathbf{w}_a = \frac{\mathbf{a}(0)}{\sqrt{N}}$. Then,

$$g(f) = \frac{|\mathbf{a}^*(f) \mathbf{a}(0)|^2}{N} \quad (24)$$

$$= \frac{1}{N} \left| \sum_{n=0}^{N-1} e^{-j2\pi \frac{f d_x u_x}{c} n} \right|^2 \quad (25)$$

$$= F_N \left(\frac{2\pi d_x u_x}{c} f \right) \quad (26)$$

with $F_N(x) = \frac{1}{N} \left(\frac{\sin \frac{Nx}{2}}{\sin \frac{x}{2}} \right)^2$. The 3-dB loss occurs when

$$F_N \left(\frac{\pi d_x u_x}{c} W \right) = \frac{N}{2}. \quad (27)$$

Given the array length $L_x = Nd_x$, the argument of $F_N(\cdot)$ above suggests defining

$$\alpha \equiv \frac{W}{f_c} \frac{L_x u_x}{\lambda} \quad (28)$$

and, indeed, this product of the normalized bandwidth and normalized projected aperture—termed *channel dispersion factor* in [27]—turns out to be an excellent measure of the squint intensity with analog beamforming and plays a central role in the sequel. With it, (27) is compacted into

$$F_N \left(\frac{\pi \alpha}{N} \right) = \frac{N}{2} \quad (29)$$

and, as $N \rightarrow \infty$, it boils down to

$$\left(\frac{\sin \frac{\pi \alpha}{2}}{\frac{\pi \alpha}{2}} \right)^2 = \frac{1}{2}, \quad (30)$$

whose numerical solution gives

$$\alpha_{3\text{dB}} \approx 0.886. \quad (31)$$

As shown in App. A, $\alpha_{3\text{dB}}$ decreases with N and the convergence to 0.886 is quick, hence this value holds virtually for any N ; the error is only 5% for $N = 3$ [30, Fig. 2.4].

Just like a 3-dB loss in gain maps to $\alpha_{3\text{dB}}$, any other loss value has its corresponding α . For any such α , as dictated by (28), the larger the bandwidth, the smaller the array must be; and the further the beam points from the broadside direction, the smaller that the bandwidth and/or the array need to be. Since, for an exact broadside orientation, there is no beam squint, it is henceforth assumed that $\alpha > 0$.

IV. APPROACHING SQUINT-FREE PERFORMANCE

In this section, a simple criterion is introduced to determine whether the beamformer is approaching squint-free performance.

A. Average Beamforming Gain

Let us define the average beamforming gain

$$g_{\text{avg}} = \frac{1}{W} \int_{-\frac{W}{2}}^{\frac{W}{2}} g(f) df \quad (32)$$

and, by means of the positive definite matrix

$$\mathbf{B} = \frac{1}{W} \int_{-\frac{W}{2}}^{\frac{W}{2}} \mathbf{a}(f) \mathbf{a}^*(f) df, \quad (33)$$

further express such average gain as [31, Eq. 20]

$$g_{\text{avg}} = \frac{1}{W} \int_{-\frac{W}{2}}^{\frac{W}{2}} \|\mathbf{a}^*(f) \mathbf{W}_a (\mathbf{W}_a^* \mathbf{W}_a)^{-\frac{1}{2}}\|^2 df \quad (34)$$

$$= \text{tr}(\mathbf{W}_a (\mathbf{W}_a^* \mathbf{W}_a)^{-1} \mathbf{W}_a^* \mathbf{B}). \quad (35)$$

Note that

$$[\mathbf{B}]_{n',n} = \frac{1}{W} \int_{-\frac{W}{2}}^{\frac{W}{2}} \exp\left(j2\pi \frac{f_c + f}{c} \mathbf{u}^\top (\mathbf{r}_n - \mathbf{r}_{n'})\right) df \quad (36)$$

and, as far as the eigenvalues of \mathbf{B} are concerned, the term

$$\exp\left(j2\pi \frac{f_c}{c} \mathbf{u}^\top (\mathbf{r}_n - \mathbf{r}_{n'})\right) \quad (37)$$

is irrelevant. Therefore, without loss of generality in terms of the eigenvalues, we can let $f_c = 0$ to obtain

$$[\mathbf{B}]_{n',n} = \frac{1}{W} \int_{-\frac{W}{2}}^{\frac{W}{2}} \exp\left(j2\pi \frac{f}{c} \mathbf{u}^\top (\mathbf{r}_n - \mathbf{r}_{n'})\right) df \quad (38)$$

$$= \frac{\sin(\pi W \mathbf{u}^\top (\mathbf{r}_n - \mathbf{r}_{n'})/c)}{\pi W \mathbf{u}^\top (\mathbf{r}_n - \mathbf{r}_{n'})/c}. \quad (39)$$

B. Simple Criterion

With fully digital beamforming, the squint can be eradicated to attain $g(f) = N$. Since $g(f) \leq N$, it follows that $g_{\text{avg}} = N$ is a necessary and sufficient condition for $g(f) = N$. Thus, $g_{\text{avg}} \approx N$ is a simple criterion to determine whether the beamformer is approaching squint-free performance.

C. Analog Beamformer Maximizing the Average Beamforming Gain

Given $\lambda_\ell(\mathbf{B})$ as the ℓ th largest eigenvalue of \mathbf{B} , and \mathbf{u}_ℓ as the corresponding unit-norm eigenvector, g_{avg} is maximized by [31, Prop. 1]

$$\mathbf{W}_a = [\mathbf{u}_0 \quad \cdots \quad \mathbf{u}_{N_{\text{RF}}-1}] \quad (40)$$

at

$$g_{\text{avg}} = \sum_{\ell < N_{\text{RF}}} \lambda_\ell(\mathbf{B}). \quad (41)$$

Note that

$$\sum_n \lambda_\ell(\mathbf{B}) = \text{tr}(\mathbf{B}) = N \quad (42)$$

consistent with the fact that an all-digital implementation ($N_{\text{RF}} = N$) incurs no beam squint.

V. LINEAR ARRAYS

Before embarking on the analysis with UPAs, let us first entertain the ULA case, i.e., for $N_y = 1$.

A. Continuous-Aperture Representation

From (41), the eigenvalues of \mathbf{B} are of great importance. For the sake of analysis, we move into the continuous realm by replacing the discrete array with a continuous one.

For linear arrays, (39) reduces to

$$[\mathbf{B}]_{n',n} = \frac{\sin(\pi W u_x d_x (n - n')/c)}{\pi W u_x d_x (n - n')/c} \quad (43)$$

$$= \frac{\sin \pi \alpha \frac{n' - n}{N}}{\pi \alpha \frac{n' - n}{N}}. \quad (44)$$

The symmetry enables us to assume $\alpha > 0$ without loss of generality. The continuous counterpart to \mathbf{B} is the integral operator [32, Sec. V]

$$B_\alpha : L^2(\mathbb{R}) \rightarrow L^2(\mathbb{R}) \quad (45)$$

$$s(r) \mapsto \int B_\alpha(r', r) s(r) dr$$

where

$$B_\alpha(r', r) = [r \in I][r' \in I] \frac{\sin(\pi \alpha (r - r'))}{\pi (r - r')} \quad (46)$$

is the kernel with $I = [-\frac{1}{2}, \frac{1}{2}]$. Here, $[\cdot]$ denotes the Iverson bracket [33]

$$[\text{condition}] \equiv \begin{cases} 1 & \text{the condition is true} \\ 0 & \text{otherwise} \end{cases}. \quad (47)$$

The matrix \mathbf{B} can be recovered from (46) by sampling at the normalized element coordinates, namely

$$[\mathbf{B}]_{n',n} = \frac{1}{\alpha} B_\alpha\left(\frac{r_{n'}}{L_x}, \frac{r_n}{L_x}\right), \quad (48)$$

where the normalization by $\frac{1}{\alpha}$ is convenient, as evidenced in subsequent sections. In terms of eigenvalues, the continuous

representation becomes exact as the spacings vanish, namely [32, Sec. V-C]

$$\frac{\alpha}{N} \lambda_\ell(\mathbf{B}) \rightarrow \lambda_\ell(\mathcal{B}_\alpha) \quad (49)$$

in two-norm as N approaches infinity.

For any α , which measures the squint intensity that would be experienced with purely analog beamforming (recall Sec. III), the squint-free condition with hybrid beamforming, $\sum_{\ell < N_{\text{RF}}} \lambda_\ell(\mathbf{B}) \approx N$, translates to

$$\sum_{\ell < N_{\text{RF}}} \lambda_\ell(\mathcal{B}_\alpha) \approx \alpha \quad (50)$$

and the counterpart to the all-digital extreme in (42) is $\sum_{\ell=0}^{\infty} \lambda_\ell(\mathcal{B}_\alpha) = \alpha$.

The continuous-aperture representation introduced herein is an analytically friendly proxy to the discrete model, and its practical relevance is confirmed by thorough numerical studies.

B. Eigenvalue Behavior

The eigenvalues of \mathcal{B}_α are well studied [34]. In particular, they are bounded above by 1 and asymptotically polarized into two levels. Precisely, as $\alpha \rightarrow \infty$,

$$|\{\ell : \lambda_\ell(\mathcal{B}_\alpha) > \epsilon\}| = \alpha + \mathcal{O}(\log \alpha) \quad (51)$$

for any $\epsilon \in (0, 1)$. Put another way, for sufficiently large α , we can informally write

$$(\lambda_0(\mathcal{B}_\alpha), \lambda_1(\mathcal{B}_\alpha), \dots) \approx (\underbrace{1, \dots, 1}_{\approx \alpha}, 0, \dots). \quad (52)$$

C. Number of Required RF chains

Let us consider the asymptotic regime where $\alpha \rightarrow \infty$ and $N_{\text{RF}} = \lceil p\alpha \rceil$ with $p > 0$ a constant. Then,

$$\sum_{\ell < N_{\text{RF}}} \lambda_\ell(\mathcal{B}_\alpha) = \min(p, 1)\alpha + o(\alpha), \quad (53)$$

which (see App. B) is a consequence of (52). Therefore,

$$\sum_{\ell < N_{\text{RF}}} \lambda_\ell(\mathcal{B}_\alpha) = \alpha + o(\alpha) \quad (54)$$

if $p \geq 1$. Recalling the squint-free condition in (50), this implies that, asymptotically, α RF chains are needed to approach squint-free performance.

D. Beam-space Architecture

An instance of the above general ULA result had been empirically observed in the context of beam-space MIMO [27], namely that the beam squint can be mitigated with $\lceil \alpha \rceil$ RF chains and a simple analog network. The ℓ th column of \mathbf{W}_a is then the MRT beamformer $\frac{\mathbf{a}(f_\ell)}{\sqrt{N}}$ for the relative frequency

$$f_\ell = \frac{c}{u_x d_x} \cdot \frac{\ell - \frac{N_{\text{RF}}-1}{2}}{N} = \frac{\ell - \frac{N_{\text{RF}}-1}{2}}{\alpha} W, \quad (55)$$

such that W is segregated into N_{RF} subbands spaced by $\frac{W}{\alpha}$. Intuitively, this narrower subbands are less susceptible

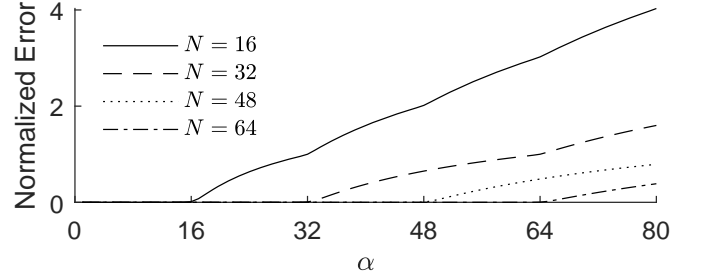


Fig. 3. Validity of the continuous-aperture representation.

to beam squint; in fact, they are dimensioned such that the squint vanishes asymptotically over each of them, with the digital stage of the beamformer taking care of the rest.

A dual interpretation, recalling (23), is that the ℓ th analog beamformer points (at its own central frequency) in direction $(1 + \frac{f_\ell}{f_c})u_x$. At the analog stage, we are therefore faced with a bank of beams arranged regularly in u_x , hence the beamspace denomination.

As the columns are orthonormal, (34) gives

$$\frac{g_{\text{avg}}}{N} = \frac{1}{NW} \int_{-\frac{W}{2}}^{\frac{W}{2}} \|\mathbf{a}^*(f) \mathbf{W}_a\|^2 df \quad (56)$$

$$= \sum_{\ell < N_{\text{RF}}} \frac{1}{W} \int_{-\frac{W}{2}}^{\frac{W}{2}} \frac{|\mathbf{a}^*(f) \mathbf{a}(f_\ell)|^2}{N^2} df. \quad (57)$$

To again move into the continuous-aperture realm, we let $N \rightarrow \infty$ while retaining the aperture, whereby

$$\begin{aligned} \frac{|\mathbf{a}^*(f) \mathbf{a}(f_\ell)|^2}{N^2} &= \left(\frac{\sin(\pi(\ell - \frac{N_{\text{RF}}-1}{2} - \frac{f}{W}\alpha))}{N \sin(\pi(\ell - \frac{N_{\text{RF}}-1}{2} - \frac{f}{W}\alpha)/N)} \right)^2 \\ &\rightarrow \left(\frac{\sin(\pi(\ell - \frac{N_{\text{RF}}-1}{2} - \frac{f}{W}\alpha))}{\pi(\ell - \frac{N_{\text{RF}}-1}{2} - \frac{f}{W}\alpha)} \right)^2 \end{aligned} \quad (58)$$

and

$$\begin{aligned} \frac{g_{\text{avg}}}{N} &\rightarrow \sum_{\ell < N_{\text{RF}}} \frac{1}{W} \int_{-\frac{W}{2}}^{\frac{W}{2}} \left(\frac{\sin(\pi(\ell - \frac{N_{\text{RF}}-1}{2} - \frac{f}{W}\alpha))}{\pi(\ell - \frac{N_{\text{RF}}-1}{2} - \frac{f}{W}\alpha)} \right)^2 df \\ &= \frac{1}{\alpha} \sum_{\ell < N_{\text{RF}}} \int_{\ell - \frac{N_{\text{RF}}-1}{2} - \frac{\alpha}{2}}^{\ell - \frac{N_{\text{RF}}-1}{2} + \frac{\alpha}{2}} \left(\frac{\sin \pi t}{\pi t} \right)^2 dt \end{aligned} \quad (59)$$

Let us again consider the asymptotic regime, $\alpha \rightarrow \infty$ and $N_{\text{RF}} = \lceil p\alpha \rceil$ with $p > 0$ a constant. It is shown in App. C that (59) converges to $\min(p, 1)$. The result is thus identical to its counterpart with the optimum eigenvectors (recall (53)), demonstrating the asymptotic optimality of the beamspace architecture.

This architecture is computationally efficient and compelling in that no amplitude tapering is required. On top of that, the normalized response at the ℓ th RF chain, given in (58), concentrates around f_ℓ such that having a much smaller bandwidth at each RF chain incurs negligible loss. With a bandwidth of $\frac{2}{\alpha}W$ per RF chain, the average beamforming gain becomes

$$\int_{-1}^1 \left(\frac{\sin \pi t}{\pi t} \right)^2 dt \approx 0.902, \quad (60)$$

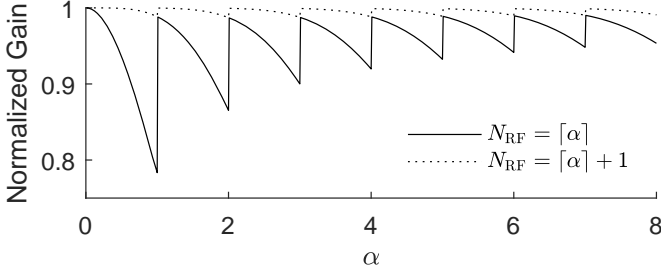


Fig. 4. Normalized gain with respect to α . The sawtooth behavior, caused by the ceiling function on the number of RF chains, quickly abates.

which falls short by only 0.45 dB. Doubling the bandwidth per RF chain shrinks this deficit to 0.22 dB.

E. Remarks

The analysis entails two limits, infinitesimal element spacing and infinite aperture-bandwidth product, and care should be exercised to preserve the relevance of the analysis to regimes of interest [35].

Recalling (49), Fig. 3 depicts the normalized approximation error for the first limit²

$$\frac{\sum_{\ell} \left(\frac{\alpha}{N} \lambda_{\ell}(\mathbf{B}) - \lambda_{\ell}(\mathbf{B}_{\alpha}) \right)^2}{\sum_{\ell} \lambda_{\ell}^2(\mathbf{B}_{\alpha})}. \quad (61)$$

The figure evidences that the continuous-aperture representation is fully valid provided that $\alpha \leq N$, a condition clearly fulfilled for any scenario of interest because

$$\alpha = N \frac{W}{f_c} \frac{d_x u_x}{\lambda} \ll N. \quad (62)$$

This leaves the second limit, base on which the analysis is valid as long as α is minimally large. Pleasingly, even for very small α this turns out to be the case. Fig. 4 depicts the normalized gain $(\sum_{\ell < N_{\text{RF}}} \lambda_{\ell}(\mathbf{B}_{\alpha}))/\alpha$ with respect to α , confirming that, for virtually any α , squint-free performance can be virtually achieved with $\lceil \alpha \rceil + 1$ RF chains.

VI. PLANAR ARRAYS

In this section, the result is extended to planar arrays; this generalization is not straightforward in that a naive separable architecture makes an inefficient use of the RF chains. For planar arrays, the intensity of beam squint can be measured by

$$\boldsymbol{\alpha} \equiv \begin{bmatrix} \alpha_x \\ \alpha_y \end{bmatrix} = \frac{W}{f_c} \begin{bmatrix} \frac{L_x u_x}{\lambda} \\ \frac{L_y u_y}{\lambda} \end{bmatrix}, \quad (63)$$

which is a natural extension of α for linear arrays.

A. Separable Architecture

Motivated by (5), separable beamformers are often considered where [9, Ch. 1.2]

$$\mathbf{W}_a = \mathbf{W}_x \otimes \mathbf{W}_y \quad (64)$$

² $\lambda_{\ell}(\mathbf{B}_{\alpha})$ can be computed via the software package `chebfun2` [36].

with $\mathbf{W}_x \in \mathbb{C}^{N_x \times N_{\text{RF},x}}$ and $\mathbf{W}_y \in \mathbb{C}^{N_y \times N_{\text{RF},y}}$, and with $N_{\text{RF}} = N_{\text{RF},x} N_{\text{RF},y}$. Then,

$$g(f) = \left\| ((\mathbf{W}_x^* \otimes \mathbf{W}_y^*)(\mathbf{W}_x \otimes \mathbf{W}_y))^{-\frac{1}{2}} \cdot (\mathbf{W}_x^* \otimes \mathbf{W}_y^*)(\mathbf{a}_x(f) \otimes \mathbf{a}_y(f)) \right\|^2 \quad (65)$$

$$= \left\| (\mathbf{W}_x^* \mathbf{W}_x)^{-\frac{1}{2}} \mathbf{W}_x^* \mathbf{a}_x(f) \otimes (\mathbf{W}_y^* \mathbf{W}_y)^{-\frac{1}{2}} \mathbf{W}_y^* \mathbf{a}_y(f) \right\|^2 \quad (66)$$

$$= \left\| (\mathbf{W}_x^* \mathbf{W}_x)^{-\frac{1}{2}} \mathbf{W}_x^* \mathbf{a}_x(f) \right\|^2 \cdot \left\| (\mathbf{W}_y^* \mathbf{W}_y)^{-\frac{1}{2}} \mathbf{W}_y^* \mathbf{a}_y(f) \right\|^2 \quad (67)$$

$$= g_x(f) g_y(f) \quad (68)$$

given

$$g_x(f) = \left\| (\mathbf{W}_x^* \mathbf{W}_x)^{-\frac{1}{2}} \mathbf{W}_x^* \mathbf{a}_x(f) \right\|^2 \quad (69)$$

$$g_y(f) = \left\| (\mathbf{W}_y^* \mathbf{W}_y)^{-\frac{1}{2}} \mathbf{W}_y^* \mathbf{a}_y(f) \right\|^2. \quad (70)$$

It follows that (see App. D)

$$\frac{g_{\text{avg}}}{N} \leq \min \left(\frac{g_{\text{avg},x}}{N_x}, \frac{g_{\text{avg},y}}{N_y} \right) \quad (71)$$

where $g_{\text{avg},x} = \frac{1}{W} \int_{-\frac{W}{2}}^{\frac{W}{2}} g_x(f) df$ and $g_{\text{avg},y} = \frac{1}{W} \int_{-\frac{W}{2}}^{\frac{W}{2}} g_y(f) df$.

Attaining $g_{\text{avg}} \approx N$ with a separable structure entails $g_{\text{avg},x} \approx N_x$ and $g_{\text{avg},y} \approx N_y$. For $u_x \neq 0$ and $u_y \neq 0$ in (3), asymptotically in the array aperture and/or the bandwidth it holds that $N_{\text{RF},x} \geq \alpha_x$ and $N_{\text{RF},y} \geq \alpha_y$ as per Sec. V. Thus,

$$N_{\text{RF}} \geq \alpha_x \alpha_y = \frac{L_x L_y u_x u_y}{c^2} W^2, \quad (72)$$

which is *quadratic* in the diagonal dimensions of the array and also quadratic in the bandwidth. In the sequel, it is shown that a nonseparable beamformer can greatly reduce this number.

B. Continuous-Aperture Representation

Again resorting to a continuous-aperture representation, the counterpart to \mathbf{B} is the integral operator

$$\mathbf{B}_{\alpha} : L^2(\mathbb{R}^2) \rightarrow L^2(\mathbb{R}^2) \quad (73)$$

$$s(\mathbf{r}) \mapsto \int \mathbf{B}_{\alpha}(\mathbf{r}', \mathbf{r}) s(\mathbf{r}) d\mathbf{r}$$

where

$$\mathbf{B}_{\alpha}(\mathbf{r}', \mathbf{r}) = [\mathbf{r} \in I^2] [\mathbf{r}' \in I^2] \frac{\sin(\pi \boldsymbol{\alpha}^{\top} (\mathbf{r} - \mathbf{r}'))}{\pi \boldsymbol{\alpha}^{\top} (\mathbf{r} - \mathbf{r}') / \|\boldsymbol{\alpha}\|} \quad (74)$$

is the kernel. The matrix \mathbf{B} can again be recovered from (74) by sampling at the normalized element coordinates, precisely

$$[\mathbf{B}]_{n',n} = \frac{1}{\|\boldsymbol{\alpha}\|} \mathbf{B}_{\alpha} \left(\begin{bmatrix} \frac{x_{n'}}{L_x} \\ \frac{y_{n'}}{L_y} \end{bmatrix}, \begin{bmatrix} \frac{x_n}{L_x} \\ \frac{y_n}{L_y} \end{bmatrix} \right). \quad (75)$$

In terms of eigenvalues, the continuous representation becomes exact as the spacings vanish, namely [32, Sec. V-C]

$$\frac{\|\boldsymbol{\alpha}\|}{N} \lambda_{\ell}(\mathbf{B}) \rightarrow \lambda_{\ell}(\mathbf{B}_{\alpha}) \quad (76)$$

in two-norm as N_x and N_y grow large with a fixed ratio. The squint-free condition is

$$\sum_{\ell < N_{\text{RF}}} \lambda_{\ell}(\mathbf{B}_{\alpha}) \approx \|\boldsymbol{\alpha}\|. \quad (77)$$

C. A Bag of Tricks

The operator \mathcal{B} obtained from the continuous-aperture representation is still ill-suited to analysis. To enable further progress, some handy results are set forth in this subsection; they allow capitalizing on ULAs asymptotics.

Let us construct a rotation matrix $\mathbf{R} \in \mathbb{R}^{2 \times 2}$ whose first row is $\frac{\boldsymbol{\alpha}}{\|\boldsymbol{\alpha}\|}$, and then rotate the axes into

$$\tilde{\mathbf{r}} = [\tilde{r}_x \ \tilde{r}_y]^\top = \mathbf{R}\mathbf{r} \quad \tilde{\mathbf{r}}' = [\tilde{r}'_x \ \tilde{r}'_y] = \mathbf{R}\mathbf{r}'. \quad (78)$$

The right-hand side of (74) can then be recast as

$$[\tilde{\mathbf{r}} \in \mathbf{R}\mathbf{I}^2][\tilde{\mathbf{r}}' \in \mathbf{R}\mathbf{I}^2] \frac{\sin(\pi\|\boldsymbol{\alpha}\|(\tilde{r}_x - \tilde{r}'_x))}{\pi(\tilde{r}_x - \tilde{r}'_x)}. \quad (79)$$

Defining the kernel

$$\begin{aligned} \tilde{B}_{\boldsymbol{\alpha}}(\tilde{r}'_x, \tilde{r}_x) &= \left(\int [\tilde{\mathbf{r}} \in \mathbf{R}\mathbf{I}^2] d\tilde{r}_y \right)^{1/2} \\ &\cdot \left(\int [\tilde{\mathbf{r}}' \in \mathbf{R}\mathbf{I}^2] d\tilde{r}'_y \right)^{1/2} \frac{\sin(\pi\|\boldsymbol{\alpha}\|(\tilde{r}_x - \tilde{r}'_x))}{\pi(\tilde{r}_x - \tilde{r}'_x)} \end{aligned} \quad (80)$$

and the corresponding operator $\tilde{\mathcal{B}}_{\boldsymbol{\alpha}} : L^2(\mathbb{R}) \rightarrow L^2(\mathbb{R})$, it is shown in App. E that the singular values of $\tilde{\mathcal{B}}_{\boldsymbol{\alpha}}$ and $\mathcal{B}_{\boldsymbol{\alpha}}$ coincide. If the factors

$$\left(\int [\tilde{\mathbf{r}} \in \mathbf{R}\mathbf{I}^2] d\tilde{r}_y \right)^{1/2} \left(\int [\tilde{\mathbf{r}}' \in \mathbf{R}\mathbf{I}^2] d\tilde{r}'_y \right)^{1/2} \quad (81)$$

are replaced by indicator functions, the above boils down to the ULA kernel. This motivates bounding these factors with scalar multiples of the indicator function and invoking the Courant min-max theorem. Precisely, $\int [\tilde{\mathbf{r}} \in \mathbf{R}\mathbf{I}^2] d\tilde{r}_y$ is a piecewise linear function connecting the points

$$(-L_1/2, 0), (-L_2/2, L_3), (L_2/2, L_3), (L_1/2, 0) \quad (82)$$

given $L_1 = (|\alpha_x| + |\alpha_y|)/\|\boldsymbol{\alpha}\|$, $L_2 = ||\alpha_x| - |\alpha_y||/\|\boldsymbol{\alpha}\|$, and $L_3 = \|\boldsymbol{\alpha}\|/\max(|\alpha_x|, |\alpha_y|)$. Also, it can be bounded as

$$\begin{aligned} \delta L_3 [\tilde{r}_x \in ((1-\delta)L_1 + \delta L_2)I] \\ \leq \int [\tilde{\mathbf{r}} \in \mathbf{R}\mathbf{I}^2] d\tilde{r}_y \leq L_3 [\tilde{r}_x \in L_1 I] \end{aligned} \quad (83)$$

where $\delta \in [0, 1]$ is a constant to be determined.

Using (83) and the fact that \mathcal{B} and $\tilde{\mathcal{B}}$ share the same eigenvalues, it is shown in App. F that

$$\delta L_3 \lambda_{\ell}(\mathcal{B}_{\alpha^{\text{lo}}}) \leq \lambda_{\ell}(\mathcal{B}_{\boldsymbol{\alpha}}) \leq L_3 \lambda_{\ell}(\mathcal{B}_{\alpha^{\text{up}}}), \quad (84)$$

where $\alpha^{\text{lo}} = \|\boldsymbol{\alpha}\|((1-\delta)L_1 + \delta L_2)$ and $\alpha^{\text{up}} = \|\boldsymbol{\alpha}\|L_1$.

D. Number of Required RF Chains

Let us consider the bandwidth $r_1 W$ and the aperture $r_2 L_x \times r_2 L_y$ where $r_1, r_2 > 0$ are constants. Then,

$$\boldsymbol{\alpha} = \frac{rW}{f_c} \begin{bmatrix} \frac{L_x u_x}{\lambda} \\ \frac{L_y u_y}{\lambda} \end{bmatrix} \quad (85)$$

depends on $r \equiv r_1 r_2$, not individually on r_1 and r_2 . With the number of RF chains at

$$N_{\text{RF}} = \lceil p\alpha^{\text{up}} \rceil, \quad (86)$$

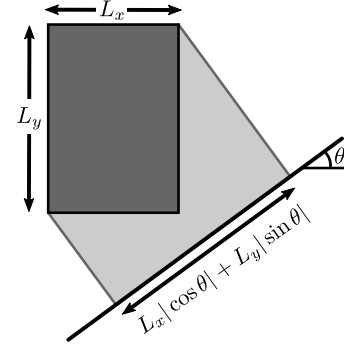


Fig. 5. Projection of the UPA onto the line parallel to $[\cos \theta \ \sin \theta]^\top$.

let us once more consider the regime $r \rightarrow \infty$. Armed with (84), it is shown in App. G that the no-squint condition

$$\sum_{\ell < N_{\text{RF}}} \lambda_{\ell}(\mathcal{B}) = \|\boldsymbol{\alpha}\| + o(r) \quad (87)$$

holds if and only if $p \geq 1$. The minimum number of RF chains that asymptotically attain squint-free performance is thus

$$\alpha^{\text{up}} = |\alpha_x| + |\alpha_y| \quad (88)$$

$$= \frac{W}{f_c} \cdot \frac{L_x |\cos \theta| + L_y |\sin \theta|}{\lambda} \sin \phi, \quad (89)$$

where $L_x |\cos \theta| + L_y |\sin \theta|$ is the projection of the UPA onto a line parallel to $[\cos \theta \ \sin \theta]^\top$ (see Fig. 5). In conjunction with $\sin \phi$, this projects the array onto the direction of beamforming as illustrated in Fig. 1.

This result can be readily generalized to non-UPA planar topologies.

E. Beamspace Architecture

A beamspace architecture analogous to the ULA one in Sec. V-D can be constructed by choosing the ℓ th column of \mathbf{W}_a as the MRT beamformer $\mathbf{a}(f_{\ell})$ for relative frequency

$$f_{\ell} = \frac{\ell - \frac{N_{\text{RF}}-1}{2}}{\alpha^{\text{up}}} W. \quad (90)$$

However, as the columns of \mathbf{W}_a are no longer orthonormal, the proof set forth for linear arrays does not carry over to show that (89) holds for planar arrays. Results in the next section support this, yet the proof is still an open issue.

VII. NUMERICAL RESULTS

To further support the relevance of the asymptotic analysis to values of interest, say for 6G or advanced WiFi systems, this section presents additional results.

A 128×128 UPA with half-wavelength spacing is considered, which would occupy only $6.4 \text{ cm} \times 6.4 \text{ cm}$ at 300 GHz. From (63), $\boldsymbol{\alpha}$ depends on the product $W \sin \phi$. Without loss of generality we can thus fix $\phi = 90^\circ$ and sweep only W . Table I lists the average beamforming gain normalized by its squint-free counterpart, $\frac{g_{\text{avg}}}{N}$, for the optimal and beamspace architectures; precisely, the listed values are the worst normalized gains over $\theta \in \{0^\circ, 1^\circ, \dots, 359^\circ\}$. The number of additional RF chains in the table is $N_{\text{RF}} - \lceil \alpha^{\text{up}} \rceil$.

TABLE I
NORMALIZED AVERAGE BEAMFORMING GAIN (WORST VALUE OVER AZIMUTH ANGLE) FOR VARIOUS SETUPS

		Bandwidth [GHz]									
# additional RF chains		1	2	3	4	5	10	15	20	25	30
Optimal	0	0.9877	0.9523	0.8984	0.8324	0.9776	0.9638	0.9680	0.9720	0.9737	0.9749
	1	1.0000	0.9993	0.9997	0.9933	0.9991	0.9961	0.9959	0.9961	0.9960	0.9959
	2	1.0000	0.9999	0.9999	0.9998	0.9998	0.9996	0.9996	0.9995	0.9994	0.9993
Beamspace	0	0.9876	0.9518	0.8963	0.8266	0.9089	0.9308	0.9431	0.9510	0.9564	0.9603
	1	0.8170	0.8349	0.8600	0.8868	0.9264	0.9405	0.9492	0.9551	0.9596	0.9631
	2	0.9952	0.9819	0.9632	0.9433	0.9531	0.9607	0.9658	0.9695	0.9722	0.9744

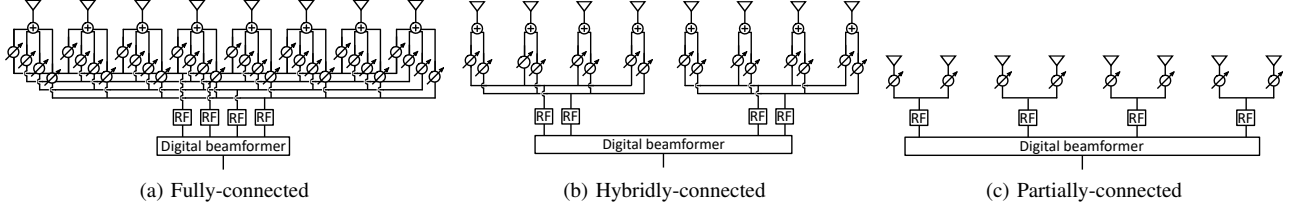


Fig. 6. Hybrid architectures: fully-connected, hybridly-connected, and partially-connected.

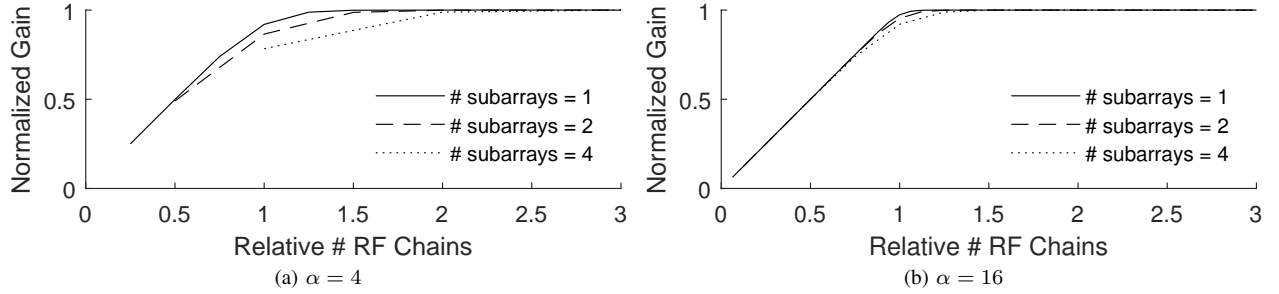


Fig. 7. Normalized beamforming gain $\frac{g_{avg}}{N}$ for a 128-element ULA. The analog beamformer maximizing the average beamforming gain is used. The relative number of RF chains for the horizontal axis is the number of RF chains normalized by the number of required RF chains, that is, $\frac{N_{RF}}{\alpha}$.

For the optimal architecture, $\lceil \alpha^{up} \rceil + 1$ RF chains ensure over 99% of the squint-free gain over the entire range and, for strong squints, $\lceil \alpha^{up} \rceil + 1$ RF chains suffice to perform almost as impressively. As of the beamspace architecture, it exhibits a remarkably small performance deficit relative to the optimal one—a deficit that can be overcome with only one or two extra RF chains. Given its simplicity, this makes it a decidedly attractive alternative.

VIII. EXTENSIONS

While the formulation hitherto has considered a general hybrid array, fully-connected as per the illustration in Fig. 6, this section turns the attention to the more restrictive hybridly-connected and partially-connected structures, and further to receivers equipped themselves with an array.

A. Hybridly-Connected Architecture

In a hybridly-connected architecture (see Fig. 6), the array is partitioned into subarrays and only a subset of the RF chains is connected to each subarray [37]. With proper antenna indexing, the analog beamforming matrix exhibits a block diagonal structure, namely

$$\mathbf{W}_a = \text{blkdiag}(\mathbf{W}_{a,0}, \dots, \mathbf{W}_{a,M-1}) \quad (91)$$

with $\mathbf{W}_{a,m}$ the analog beamformer for the m th subarray and M the number of subarrays. Plugging (91) into (12) gives

$$g(f) = \left\| \mathbf{a}^*(f) \text{blkdiag}(\mathbf{W}_{a,0}(\mathbf{W}_{a,0}^* \mathbf{W}_{a,0})^{-\frac{1}{2}}, \dots, \mathbf{W}_{a,M-1}(\mathbf{W}_{a,M-1}^* \mathbf{W}_{a,M-1})^{-\frac{1}{2}}) \right\|^2 \quad (92)$$

$$= \sum_m g_m(f) \quad (93)$$

where

$$g_m(f) = \left\| \mathbf{a}_m^*(f) \mathbf{W}_{a,m}(\mathbf{W}_{a,m}^* \mathbf{W}_{a,m})^{-\frac{1}{2}} \right\|^2 \quad (94)$$

given $\mathbf{a}_m(f)$ as the channel for the m th subarray. Therefore,

$$g_{avg} = \sum_m g_{avg,m} \quad (95)$$

where

$$g_{avg,m} = \frac{1}{W} \int_{-\frac{W}{2}}^{\frac{W}{2}} g_m(f) df. \quad (96)$$

The behavior of a hybridly-connected array can thus be broken down into that of the subarrays, and the squint-free criterion is $g_{avg,m}$ approximately equaling the number of elements in the m th subarray for every m .

Let us first consider an N -element ULA composed of M subarrays in the asymptotic regime. Each subarray is

connected to $\frac{N_{\text{RF}}}{M}$ RF chains. From Sec. V, squint-free performance requires

$$\frac{N_{\text{RF}}}{M} \geq \frac{\alpha}{M} \Leftrightarrow N_{\text{RF}} \geq \alpha, \quad (97)$$

as in the fully-connected architecture. This is remarkable given the M -fold savings in number of phase shifters, yet the asymptotic regime is now determined by $\frac{\alpha}{M} \rightarrow \infty$, whose convergence rate is slower (see Fig. 7).

The situation changes with planar arrays. Let us consider an $N_x \times N_y$ UPA composed of $M_x \times M_y$ subarrays. The asymptotic regime of interest is the one considered in Sec. VI with fixed M_x and M_y . Each subarray is then connected to $\frac{N_{\text{RF}}}{M_x M_y}$ RF chains. Attaining squint-free performance requires

$$\frac{N_{\text{RF}}}{M_x M_y} \geq \frac{|\alpha_x|}{M_x} + \frac{|\alpha_y|}{M_y} \Leftrightarrow N_{\text{RF}} \geq M_y |\alpha_x| + M_x |\alpha_y|, \quad (98)$$

which is at least $\min(M_x, M_y)$ -times larger than the number of RF chains required by the fully-connected case.

B. Partially-Connected Architecture

With a single RF chain per subarray, a partially-connected array is the simplest instance of a hybridly-connected architecture (see Fig. 6). As per (95), the behavior of a hybrid array with a partially-connected analog network can be decomposed into that of the subarrays.

Consider an N -element ULA composed of $M = N_{\text{RF}}$ subarrays with identical subarray beamformer $\mathbf{w}_a \in \mathbb{C}^{\frac{N}{M}}$. As per (95), $g_{\text{avg}} = M g_{\text{avg},0}$. Two subarray beamformers are considered, the MRT beamformer and the optimal beamformer, both implementable with a single RF chain and M delay lines (see App. H).

For the MRT beamformer,

$$g_{\text{avg}} = \frac{M}{W} \int_{-\frac{W}{2}}^{\frac{W}{2}} F_{\frac{N}{M}} \left(\frac{2\pi d_x u_x}{c} f \right) df \quad (99)$$

and thus

$$\frac{g_{\text{avg}}}{N} \rightarrow \frac{1}{W} \int_{-\frac{W}{2}}^{\frac{W}{2}} \left(\frac{\sin(\frac{\pi L_x u_x}{Mc} f)}{\frac{\pi L_x u_x}{Mc} f} \right)^2 df \quad (100)$$

$$= \frac{M}{\pi \alpha} \int_{-\frac{\pi \alpha}{2M}}^{\frac{\pi \alpha}{2M}} \left(\frac{\sin t}{t} \right)^2 dt \quad (101)$$

$$= \frac{2M}{\pi \alpha} \left(\text{Si} \left(\frac{\pi \alpha}{M} \right) - \frac{\sin^2 \frac{\pi \alpha}{2M}}{\frac{\pi \alpha}{2M}} \right) \quad (102)$$

as the array densifies; here, $\text{Si}(\cdot)$ is the sine integral.

Let us now consider the optimal beamformer in terms of average beamforming gain. As array densifies, as per (49),

$$\frac{g_{\text{avg}}}{N} \rightarrow \frac{\lambda_0(\mathcal{B}_{\alpha/M})}{\alpha/M}. \quad (103)$$

Fig. 8 compares the normalized average beamforming gain for fully- and partially-connected architectures. Recalling (53), the asymptotic result $\min(p, 1)$ is plotted for the fully-connected architecture while (102) and (103) are plotted for the partially-connected architecture.

Although the squint cannot be completely eradicated with a partially-connected architecture, it is rather enticing because

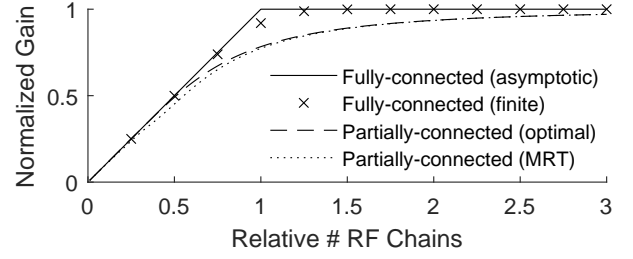


Fig. 8. Comparison of array architectures. For the fully-connected architecture, $\alpha \rightarrow \infty$ and $\alpha = 4$ are considered. The relative number of RF chains for the horizontal axis is the number of RF chains normalized by the number of required RF chains, that is, $\frac{N_{\text{RF}}}{\alpha}$. This equals $\frac{M}{\alpha}$ for partially-connected architectures.

of the M -fold save in the number of phase shifters. For instance, with $M = \alpha, 2\alpha, 3\alpha$, a partially-connected architecture incurs respective losses of only 1.11, 0.29, 0.13 dB, even with simple MRT beamforming; in Fig. 8, these losses can be appreciated in linear scale.

Similar to their hybridly-connected brethren, partially-connected architectures become less alluring with planar arrays. To maintain the subarray size, one needs the scalings

$$M_x \propto \alpha_x \quad M_y \propto \alpha_y, \quad (104)$$

whereby the substantial disadvantage of the separable architecture in Sec. VI-A is reproduced. This shortcoming can be alleviated by a use of dynamic subarrays [31], but at the expense of additional hardware complexity.

C. Multiantenna Receiver

The separable property of far-field LOS multiantenna channels enables the extension to such a setting too. Positing an N_t -element transmitter and an N_r -element receiver, the LOS channel can be expressed as [38, Sec. II-A]

$$\mathbf{H}(f) = \mathbf{a}_r(f) \mathbf{a}_t^*(f) \quad (105)$$

where $\mathbf{a}_t(f) \in \mathbb{C}^{N_t}$ is the normalized channel between the transmit array and the receive array center, and reciprocally for $\mathbf{a}_r(f) \in \mathbb{C}^{N_r}$. The squint-free condition is $g_{\text{avg}} \approx N_t N_r$.

Let us denote the analog and digital beamformers by $\mathbf{W}_{a,t}$ and $\mathbf{w}_{d,t}(f)$ for the transmitter, and $\mathbf{W}_{a,r}$ and $\mathbf{w}_{d,r}(f)$ for the receiver. An analogous signal model to that in Sec. II-C is

$$y(f) = \mathbf{w}_{d,r}^*(f) \mathbf{W}_{a,r}^* (\mathbf{H}(f) \mathbf{W}_{a,t} \mathbf{w}_{d,t}(f) s(f) + \mathbf{v}(f)) \quad (106)$$

where each entry of $\mathbf{v}(f)$ describes a white Gaussian noise process with unit power spectral density. Letting $s(f)$ have unit power, the power constraint becomes

$$\frac{1}{W} \int_{-\frac{W}{2}}^{\frac{W}{2}} \|\mathbf{W}_{a,t} \mathbf{w}_{d,t}(f)\|^2 df = \text{SNR}. \quad (107)$$

Also, without loss of generality, we let $\|\mathbf{W}_{a,r} \mathbf{w}_{d,r}(f)\| = 1$.

Reiterating the simplifications made in Sec. II-C gives

$$y(f) = \sqrt{g(f)p(f)} s(f) + \mathbf{W}_{a,r}^* \mathbf{w}_{d,r}^*(f) \mathbf{v}(f) \quad (108)$$

where

$$g(f) = \|\mathbf{w}_{d,r}^*(f) \mathbf{W}_{a,r}^* \mathbf{H}(f) \mathbf{W}_{a,t} \mathbf{w}_{d,t}(f)\|^2 \quad (109)$$

$$= |\mathbf{a}_t^*(f) \mathbf{W}_{a,t} \mathbf{w}_{d,t}(f)|^2 \cdot |\mathbf{a}_r^*(f) \mathbf{W}_{a,r} \mathbf{w}_{d,r}(f)|^2 \quad (110)$$

$$= g_t(f) g_r(f) \quad (111)$$

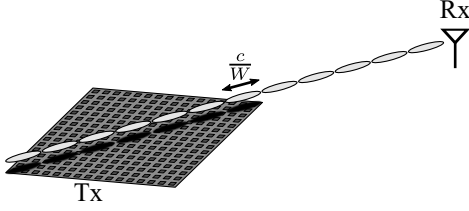


Fig. 9. A train of symbols, each of length $\frac{c}{W}$, traveling over the array along the worst possible direction in terms of the symbol delay across element.

with

$$g_t(f) = |\mathbf{a}_t^*(f) \mathbf{W}_{a,t} \mathbf{w}_{d,t}(f)|^2 \quad (112)$$

$$g_r(f) = |\mathbf{a}_r^*(f) \mathbf{W}_{a,r} \mathbf{w}_{d,r}(f)|^2. \quad (113)$$

The effective noise $\mathbf{W}_{a,r}^* \mathbf{w}_{d,r}^*(f) v(f)$ is a white Gaussian process with unit power spectral density.

Recalling the definition of average beamforming gain in (32), it is shown in App. D that

$$\frac{g_{avg,t}}{N_t} + \frac{g_{avg,r}}{N_r} - 1 \leq \frac{g_{avg}}{N_t N_r} \leq \min\left(\frac{g_{avg,t}}{N_t}, \frac{g_{avg,r}}{N_r}\right). \quad (114)$$

From this result, plus $g_{avg,t} \leq N_t$ and $g_{avg,r} \leq N_r$, it follows that $\frac{g_{avg,t}}{N_t} = \frac{g_{avg,r}}{N_r} = 1$ is a necessary and sufficient condition for $\frac{g_{avg}}{N_t N_r} = 1$. This implies that both $g_{avg,t} \approx N_t$ and $g_{avg,r} \approx N_r$ are needed to ensure $g_{avg} \approx N_t N_r$, and vice versa, whereby the multiantenna problem is seen to decouple into two problems that have already been addressed.

IX. CONCLUSION

The main takeaway point of this work is that hybrid arrays can operate free of beam squint, just like digital arrays, only with a much smaller number of RF chains. Although derived asymptotically in the bandwidth-aperture product, this result applies for virtually any value of that product.

For a hybrid linear array designed to beamform in any direction, the needed number of RF chains is $\frac{1}{c}WL$. In contrast, a digital array requires a chain per antenna, which for half-wavelength element spacing amounts to $\frac{L}{\lambda/2} = \frac{2}{c}f_c L$. The contrast between the two expressions evidences something fundamental, namely that it is the bandwidth rather than the carrier frequency that matters to the beam squint. Indeed, $\frac{c}{W}$ is roughly the spatial length of a symbol, and squint arises once symbols cease to be much longer than the array (see Fig. 9). The value $\frac{1}{c}WL$ equals the number of symbols that fit on the array along the worst possible direction, and using that many RF chains ensures one digital sample per symbol.

For planar arrays, the ratio between the RF chains required by digital and hybrid arrays is even more pronounced, as planar arrays can use space more efficiently [20].

Notably, the above points remain valid for suboptimum beamspace architectures, and in the case of linear arrays even for hybridly-connected structures, with the concomitant reduction in number of phase shifters; for hybridly-connected planar arrays, the reduction in phase shifters entails a tradeoff with the increase in RF chains.

Further research is required to determine whether similar behaviors are encountered in multipath channels, with intelligent surfaces [39], in hybrid architectures with true-time-delay [15], [26], [40], [41], or in near-field situations [42].

APPENDIX A

As the smallest solution to (29) lies within the main lobe, it suffices to consider $0 < \alpha_{3dB} < 2$ and the problem reduces to

$$\frac{\sin \frac{\pi \alpha_{3dB}}{2}}{N \sin \frac{\pi \alpha_{3dB}}{2N}} = \frac{1}{\sqrt{2}}. \quad (115)$$

Manipulating the left-hand side into

$$\frac{\sin \frac{\pi \alpha_{3dB}}{2}}{N \sin \frac{\pi \alpha_{3dB}}{2N}} = \frac{\sin \frac{\pi \alpha_{3dB}}{2}}{\frac{\pi \alpha_{3dB}}{2}} \cdot \frac{\frac{\pi \alpha_{3dB}}{2N}}{\sin \frac{\pi \alpha_{3dB}}{2N}} \quad (116)$$

shows that it is decreasing in N . Paired with the fact that the left-hand side is decreasing in α_{3dB} , the solution of (115) is decreasing with respect to N .

APPENDIX B

Combining $\lambda_\ell(\mathcal{B}_\alpha) \leq 1$ and $\sum_\ell \lambda_\ell(\mathcal{B}_\alpha) = \alpha$, we have that

$$\sum_{\ell < N_{RF}} \lambda_\ell(\mathcal{B}_\alpha) \leq \min(p, 1)\alpha. \quad (117)$$

In turn, for $\epsilon > 0$, we also have that

$$\sum_{\ell < N_{RF}} \lambda_\ell(\mathcal{B}_\alpha) > \epsilon |\{\ell : \sigma_\ell > \epsilon, \ell < N_{RF}\}| \quad (118)$$

$$= \epsilon \min(\alpha + \mathcal{O}(\log \alpha), \lceil p\alpha \rceil) \quad (119)$$

where the last equality follows from (51). Consequently

$$\liminf_{\alpha \rightarrow \infty} \frac{\sum_{\ell < N_{RF}} \lambda_\ell(\mathcal{B}_\alpha)}{\alpha} \geq \epsilon \liminf_{\alpha \rightarrow \infty} \frac{\min(\alpha + \mathcal{O}(\log \alpha), \lceil p\alpha \rceil)}{\alpha} \quad (120)$$

$$= \epsilon \min(p, 1). \quad (121)$$

where, as the existence of the limit is not guaranteed at this point, limit inferior was used.

For ϵ arbitrarily close to 1,

$$\liminf_{\alpha \rightarrow \infty} \frac{\sum_{\ell < N_{RF}} \lambda_\ell(\mathcal{B}_\alpha)}{\alpha} = \min(p, 1). \quad (122)$$

From (117), the limit inferior and limit superior coincide, hence the limit does exist and it equals $\min(p, 1)$ as desired.

APPENDIX C

From $\int_{-\infty}^{\infty} \left(\frac{\sin \pi t}{\pi t}\right)^2 dt = 1$, which is straightforward from Parseval's identity,

$$\frac{1}{\alpha} \sum_{\ell < \lceil p\alpha \rceil} \int_{\ell - \frac{\lceil p\alpha \rceil - 1}{2} - \frac{\alpha}{2}}^{\ell - \frac{\lceil p\alpha \rceil - 1}{2} + \frac{\alpha}{2}} \left(\frac{\sin \pi t}{\pi t}\right)^2 dt \leq \frac{\lceil p\alpha \rceil}{\alpha}. \quad (123)$$

Also, it can be readily shown that

$$\begin{aligned} \frac{1}{\alpha} \sum_{\ell < \lceil p\alpha \rceil} \int_{\ell - \frac{\lceil p\alpha \rceil - 1}{2} - \frac{\alpha}{2}}^{\ell - \frac{\lceil p\alpha \rceil - 1}{2} + \frac{\alpha}{2}} \left(\frac{\sin \pi t}{\pi t}\right)^2 dt \\ \leq \frac{1}{\alpha} \sum_{\ell} \int_{\ell - \frac{\lceil p\alpha \rceil - 1}{2} - \frac{\alpha}{2}}^{\ell - \frac{\lceil p\alpha \rceil - 1}{2} + \frac{\alpha}{2}} \left(\frac{\sin \pi t}{\pi t}\right)^2 dt \end{aligned} \quad (124)$$

$$= \frac{1}{\alpha} \cdot \alpha \int_{-\infty}^{\infty} \left(\frac{\sin \pi t}{\pi t}\right)^2 dt = 1. \quad (125)$$

$$\begin{aligned} & \frac{1}{\alpha} \sum_{\ell < \lceil p\alpha \rceil} \int_{\ell - \frac{\lceil p\alpha \rceil - 1}{2} - \frac{\alpha}{2}}^{\ell - \frac{\lceil p\alpha \rceil - 1}{2} + \frac{\alpha}{2}} \left(\frac{\sin \pi t}{\pi t} \right)^2 dt \\ & \geq \frac{1}{\alpha} \sum_{\ell} [0 \leq \ell < \lceil p\alpha \rceil] \left[\ell - \frac{\lceil p\alpha \rceil - 1}{2} + \frac{\alpha}{2} > \epsilon\alpha \right] \left[\ell - \frac{\lceil p\alpha \rceil - 1}{2} - \frac{\alpha}{2} < -\epsilon\alpha \right] \int_{\ell - \frac{\lceil p\alpha \rceil - 1}{2} - \frac{\alpha}{2}}^{\ell - \frac{\lceil p\alpha \rceil - 1}{2} + \frac{\alpha}{2}} \left(\frac{\sin \pi t}{\pi t} \right)^2 dt \end{aligned} \quad (127)$$

$$\geq \frac{1}{\alpha} \sum_{\ell} [0 \leq \ell < \lceil p\alpha \rceil] \left[\ell - \frac{\lceil p\alpha \rceil - 1}{2} + \frac{\alpha}{2} > \epsilon\alpha \right] \left[\ell - \frac{\lceil p\alpha \rceil - 1}{2} - \frac{\alpha}{2} < -\epsilon\alpha \right] \int_{-\epsilon\alpha}^{\epsilon\alpha} \left(\frac{\sin \pi t}{\pi t} \right)^2 dt \quad (128)$$

$$= \left(\frac{1}{\alpha} \sum_{\ell} [0 \leq \ell < \lceil p\alpha \rceil] \left[\ell - \frac{\lceil p\alpha \rceil - 1}{2} + \frac{\alpha}{2} > \epsilon\alpha \right] \left[\ell - \frac{\lceil p\alpha \rceil - 1}{2} - \frac{\alpha}{2} < -\epsilon\alpha \right] \right) \int_{-\epsilon\alpha}^{\epsilon\alpha} \left(\frac{\sin \pi t}{\pi t} \right)^2 dt \quad (129)$$

$$\rightarrow \min\left(p, \frac{1+p-\epsilon}{2}\right) - \max\left(0, \frac{-1+p+\epsilon}{2}\right) \quad (130)$$

Combining them, we obtain

$$\limsup_{\alpha \rightarrow \infty} \frac{1}{\alpha} \sum_{\ell < \lceil p\alpha \rceil} \int_{\ell - \frac{\lceil p\alpha \rceil - 1}{2} - \frac{\alpha}{2}}^{\ell - \frac{\lceil p\alpha \rceil - 1}{2} + \frac{\alpha}{2}} \left(\frac{\sin \pi t}{\pi t} \right)^2 dt \leq \min(p, 1). \quad (126)$$

At the same time, for $\epsilon > 0$ we can manipulate (59) as in (127)–(130), where (127) arises by imposing additional constraint on the summation index, (128) by restricting the interval of integration, (129) by factoring out the constant term with respect to the summation index, and (130) by computing the limit. Hence,

$$\begin{aligned} & \liminf_{\alpha \rightarrow \infty} \frac{1}{\alpha} \sum_{\ell < \lceil p\alpha \rceil} \int_{\ell - \frac{\lceil p\alpha \rceil - 1}{2} - \frac{\alpha}{2}}^{\ell - \frac{\lceil p\alpha \rceil - 1}{2} + \frac{\alpha}{2}} \left(\frac{\sin \pi t}{\pi t} \right)^2 dt \\ & \geq \min\left(p, \frac{1+p-\epsilon}{2}\right) - \max\left(0, \frac{-1+p+\epsilon}{2}\right). \end{aligned} \quad (131)$$

For an arbitrarily small $\epsilon > 0$,

$$\begin{aligned} & \liminf_{\alpha \rightarrow \infty} \frac{1}{\alpha} \sum_{\ell < \lceil p\alpha \rceil} \int_{\ell - \frac{\lceil p\alpha \rceil - 1}{2} - \frac{\alpha}{2}}^{\ell - \frac{\lceil p\alpha \rceil - 1}{2} + \frac{\alpha}{2}} \left(\frac{\sin \pi t}{\pi t} \right)^2 dt \\ & \geq \min\left(p, \frac{1+p}{2}\right) - \max\left(0, \frac{-1+p}{2}\right) = \min(p, 1), \end{aligned} \quad (132)$$

which concludes the proof.

APPENDIX D

This appendix identifies the maximum and minimum of

$$\frac{1}{W} \int_{-\frac{W}{2}}^{\frac{W}{2}} \frac{g_t(f)g_r(f)}{N_t N_r} df \quad (133)$$

under the constraints

$$\begin{aligned} 0 \leq g_t(f) \leq N_t \quad & \frac{1}{W} \int_{-\frac{W}{2}}^{\frac{W}{2}} g_t(f) df = g_{\text{avg},t} \\ 0 \leq g_r(f) \leq N_r \quad & \frac{1}{W} \int_{-\frac{W}{2}}^{\frac{W}{2}} g_r(f) df = g_{\text{avg},r}. \end{aligned} \quad (134)$$

Introducing

$$f_t(t) \equiv \frac{g_t(W(t - \frac{1}{2}))}{N_t} \quad f_r(t) \equiv \frac{g_r(W(t - \frac{1}{2}))}{N_r}, \quad (135)$$

the objective and the constraints become

$$\int_0^1 f_t(t)f_r(t)df \quad (136)$$

and

$$\begin{aligned} 0 \leq f_t(t) \leq 1 \quad & \int_0^1 f_t(t)df = g_{\text{avg},t} \\ 0 \leq f_r(t) \leq 1 \quad & \int_0^1 f_r(t)df = g_{\text{avg},r}. \end{aligned} \quad (137)$$

Commencing with the maximum value,

$$\int_0^1 f_t(t)f_r(t)dt \leq \int_0^1 f_t(t)dt = g_{\text{avg},t}. \quad (138)$$

Repeating the argument gives

$$\int_0^1 f_t(t)f_r(t)dt \leq \int_0^1 f_r(t)dt = g_{\text{avg},r}. \quad (139)$$

Combining the bounds,

$$\int_0^1 f_t(t)f_r(t)dt \leq \min(g_{\text{avg},t}, g_{\text{avg},r}) \quad (140)$$

This bound is tight in that it can be attained by

$$f_t(t) = [0 \leq t \leq g_{\text{avg},t}] \quad f_r(t) = [0 \leq t \leq g_{\text{avg},r}]. \quad (141)$$

Turning to the minimum value, it can be obtained from the observation that

$$\int_0^1 (1 - f_t(t))(1 - f_r(t))dt \geq 0, \quad (142)$$

which is equivalent to

$$\int_0^1 f_t(t)f_r(t)dt \geq g_{\text{avg},t} + g_{\text{avg},r} - 1. \quad (143)$$

Together with the nonnegativity, we have that

$$\int_0^1 f_t(t)f_r(t)dt \geq \max(g_{\text{avg},t} + g_{\text{avg},r} - 1, 0). \quad (144)$$

This bound can be attained by

$$f_t(t) = [0 \leq t \leq g_{\text{avg},t}] \quad f_r(t) = [1 - g_{\text{avg},r} \leq t \leq 1]. \quad (145)$$

APPENDIX E

Let us consider a spectral decomposition of \tilde{B}_α ,

$$\tilde{B}_\alpha(\tilde{r}'_x, \tilde{r}_x) = \sum_{\ell} \lambda_{\ell} u_{\ell}(\tilde{r}'_x) \overline{u_{\ell}(\tilde{r}_x)}, \quad (146)$$

where $\{u_{\ell}\}$ is a set of orthonormal functions. Multiplying both sides with

$$\frac{[\tilde{r} \in \mathbf{RA}]}{(\int [\tilde{r} \in \mathbf{RA}] d\tilde{r}_y)^{\frac{1}{2}}} \cdot \frac{[\tilde{r}' \in \mathbf{RA}]}{(\int [\tilde{r}' \in \mathbf{RA}] d\tilde{r}'_y)^{\frac{1}{2}}}, \quad (147)$$

the left- and right-hand sides of (146) become respectively (79) and

$$\sum_{\ell} \lambda_{\ell} \tilde{u}_{\ell}(\tilde{r}') \overline{\tilde{u}_{\ell}(\tilde{r})}, \quad (148)$$

where

$$\tilde{u}_{\ell}(\tilde{r}) = \frac{[\tilde{r} \in \mathbf{RA}]}{(\int [\tilde{r} \in \mathbf{RA}] d\tilde{r}_y)^{\frac{1}{2}}} u_{\ell}(\tilde{r}_x). \quad (149)$$

We can easily verify the orthonormality of (149) from

$$\iint \frac{[\tilde{r} \in \mathbf{RA}]}{\int [\tilde{r} \in \mathbf{RA}] d\tilde{r}_y} u_{\ell}(\tilde{r}_x) \overline{u_{\ell'}(\tilde{r}_x)} d\tilde{r}_x d\tilde{r}_y \quad (150)$$

$$= \int \left(\int \frac{[\tilde{r} \in \mathbf{RA}]}{\int [\tilde{r} \in \mathbf{RA}] d\tilde{r}_y} d\tilde{r}_y \right) u_{\ell}(\tilde{r}_x) \overline{u_{\ell'}(\tilde{r}_x)} d\tilde{r}_x \quad (151)$$

$$= \int u_{\ell}(\tilde{r}_x) \overline{u_{\ell'}(\tilde{r}_x)} d\tilde{r}_x, \quad (152)$$

implying that (148) is a spectral decomposition of \tilde{B}_α . Thus, $\{\lambda_{\ell}\}$, the eigenvalues of \tilde{B}_α , are also the eigenvalues of B_α .

APPENDIX F

Consider a general statement. Let \mathcal{L} be a positive semi-definite Hilbert-Schmidt operator with kernel $L(t, t')$ and let \mathcal{G} be an operator satisfying $(\mathcal{G}s)(t) = g(t)s(t)$ with $g \in L^2(\mathbb{R})$ and $0 \leq |g(t)| \leq 1$ for all t . We wish to prove that

$$\lambda_{\ell}(\mathcal{G}\mathcal{L}\mathcal{G}) \leq \lambda_{\ell}(\mathcal{L}). \quad (153)$$

The min-max theorem for matrices [43, Thm. 4.2.6], which can be naturally generalized to self-adjoint Hilbert-Schmidt operators, does the trick. Applying it, it can be seen that

$$\lambda_{\ell}(\mathcal{G}\mathcal{L}\mathcal{G}) = \min_{\varphi \in \text{span}(\psi_0, \dots, \psi_{\ell}), \varphi \neq 0} \frac{\langle \mathcal{G}\mathcal{L}\mathcal{G}\varphi, \varphi \rangle}{\langle \varphi, \varphi \rangle} \quad (154)$$

$$= \min_{\varphi \in \text{span}(\psi_0, \dots, \psi_{\ell}), \varphi \neq 0} \frac{\langle \mathcal{L}\mathcal{G}\varphi, \mathcal{G}\varphi \rangle}{\langle \varphi, \varphi \rangle} \quad (155)$$

$$\leq \min_{\tilde{\varphi} \in \text{span}(\mathcal{G}\psi_0, \dots, \mathcal{G}\psi_{\ell}), \tilde{\varphi} \neq 0} \frac{\langle \mathcal{L}\tilde{\varphi}, \tilde{\varphi} \rangle}{\langle \tilde{\varphi}, \tilde{\varphi} \rangle} \quad (156)$$

$$\leq \max_{\dim(S)=\ell+1} \min_{\tilde{\varphi} \in S, \tilde{\varphi} \neq 0} \frac{\langle \mathcal{L}\tilde{\varphi}, \tilde{\varphi} \rangle}{\langle \tilde{\varphi}, \tilde{\varphi} \rangle} \quad (157)$$

$$= \lambda_{\ell}(\mathcal{L}), \quad (158)$$

where ψ_k is the eigenvector of $\mathcal{G}\mathcal{L}\mathcal{G}$ corresponding to the k th largest eigenvalue. The first inequality follows from the substitution $\tilde{\varphi} = \mathcal{G}\varphi$ and $\|\tilde{\varphi}\| \leq \|\varphi\|$.

APPENDIX G

This appendix proves that (87) holds if and only if $p \geq 1$.

A. Sufficiency

The sufficiency requires (87) to vanish if $p \geq 1$. Using (53) and (84),

$$\sum_{\ell \geq \lceil p\alpha^{\text{up}} \rceil} \lambda_{\ell}(\mathcal{B}_\alpha) \leq L_3 \sum_{\ell \geq \lceil p\alpha^{\text{up}} \rceil} \lambda_{\ell}(\mathcal{B}_{\alpha^{\text{up}}}) \quad (159)$$

$$= L_3 \alpha^{\text{up}} (1-p)^+ + o(r). \quad (160)$$

Therefore,

$$\frac{\sum_{\ell \geq \lceil p\alpha^{\text{up}} \rceil} \lambda_{\ell}(\mathcal{B}_\alpha)}{\sum_{\ell} \lambda_{\ell}(\mathcal{B}_\alpha)} \leq \frac{L_3 \alpha^{\text{up}} (1-p)^+ + o(r)}{\|\alpha\|} \quad (161)$$

which does converge to zero if $p \geq 1$. Recall that $\frac{\alpha^{\text{up}}}{\|\alpha\|}$ is constant with respect to r .

B. Necessity

The necessity requires (87) not to vanish for $p < 1$. From (53) and (84),

$$\frac{\sum_{\ell \geq \lceil p\alpha^{\text{up}} \rceil} \lambda_{\ell}(\mathcal{B}_\alpha)}{\sum_{\ell} \lambda_{\ell}(\mathcal{B}_\alpha)} \geq \frac{\delta L_3 \alpha^{\text{lo}} (1 - \frac{\alpha^{\text{up}}}{\alpha^{\text{lo}}} p)^+ + o(r)}{\|\alpha\|}. \quad (162)$$

Recall that both $\frac{\alpha^{\text{lo}}}{\|\alpha\|}$ and $\frac{\alpha^{\text{up}}}{\alpha^{\text{lo}}}$ are constant with respect to r . From $p < 1$, a small enough $\delta > 0$ can be chosen such that

$$\frac{\alpha^{\text{up}}}{\alpha^{\text{lo}}} p = \frac{L_1}{(1-\delta)L_1 + \delta L_2} p < 1. \quad (163)$$

Therefore, (162) cannot vanish.

APPENDIX H

One welcome property of a partially-connected architecture is that, if the subarrays are identical, both in topology and in the number of phase shifts, one can replace their individual RF chains with delay lines and connect all of them to a single RF chain without loss in performance. While the result for linear arrays with MRT beamformer can be found in [10, Sec. I-B] (also in [25, Prop. 1] and [26, Sec. III-D]), this appendix extends the result for completeness.

Precisely, the first condition corresponds to

$$\mathbf{a}_m^*(f) = \exp\left(j2\pi \frac{f_c + f}{c} \mathbf{u}^\top \bar{\mathbf{r}}_m\right) \mathbf{a}_0^*(f) \quad (164)$$

where $\bar{\mathbf{r}}_m$ is the displacement of the m th subarray with respect to the 0th one (recall (4)). The second condition is

$$\mathbf{W}_a = \text{blkdiag}(\mathbf{w}_a, \dots, \mathbf{w}_a) \quad (165)$$

where $\mathbf{w}_a \in \mathbb{C}^{\frac{N}{M}}$ is the subarray beamformer.

From the block diagonal structure (165), the beamforming gain in (12) is reduced to

$$g(f) = \frac{|\sum_m \mathbf{a}_m^*(f) [\mathbf{w}_d(f)]_m \mathbf{w}_a|^2}{\|\mathbf{w}_a\|^2 \|\mathbf{w}_d(f)\|^2}, \quad (166)$$

Armed with (164), it can be recast as

$$\frac{|\sum_m \exp(j2\pi \frac{f_c + f}{c} \mathbf{u}^\top \bar{\mathbf{r}}_m) [\mathbf{w}_d(f)]_m|^2}{\|\mathbf{w}_d(f)\|^2} \cdot \frac{|\mathbf{a}_0^*(f) \mathbf{w}_a|^2}{\|\mathbf{w}_a\|^2}. \quad (167)$$

Applying the Cauchy-Schwarz inequality,

$$g(f) \leq M g_0(f), \quad (168)$$

and the equality is seen to be attained by

$$[w_d(f)]_m = \exp\left(-j2\pi \frac{f_c + f}{c} \mathbf{u}^\top \bar{\mathbf{r}}_m\right), \quad (169)$$

which can be implemented with delay lines. This maximum beamforming gain equals (95), obtained with M RF chains.

The resulting architecture with delay lines mitigates the beam squint across the subarrays. The remainder, the beam squint within the subarray, is relatively negligible. This very idea has recently applied to a multipath setting in [25], [26].

REFERENCES

- [1] H. Do, S. Cho, J. Park, H.-J. Song, N. Lee, and A. Lozano, "Terahertz line-of-sight MIMO communication: Theory and practical challenges," *IEEE Commun. Mag.*, vol. 59, no. 3, pp. 104–109, 2021.
- [2] F. Boccardi, R. W. Heath, A. Lozano, T. L. Marzetta, and P. Popovski, "Five disruptive technology directions for 5G," *IEEE Commun. Mag.*, vol. 52, no. 2, pp. 74–80, 2014.
- [3] J. G. Andrews, S. Buzzi, W. Choi, S. V. Hanly, A. Lozano, A. C. Soong, and J. C. Zhang, "What will 5G be?" *IEEE J. Sel. Areas Commun.*, vol. 32, no. 6, pp. 1065–1082, 2014.
- [4] S. Rangan, T. S. Rappaport, and E. Erkip, "Millimeter-wave cellular wireless networks: Potentials and challenges," *Proc. IEEE*, vol. 102, no. 3, pp. 366–385, 2014.
- [5] A. L. Swindlehurst, E. Ayanoglu, P. Heydari, and F. Capolino, "Millimeter-wave massive MIMO: The next wireless revolution?" *IEEE Commun. Mag.*, vol. 52, no. 9, pp. 56–62, 2014.
- [6] X. Zhang, A. F. Molisch, and S.-Y. Kung, "Variable-phase-shift-based RF-baseband codesign for MIMO antenna selection," *IEEE Trans. Signal Process.*, vol. 53, no. 11, pp. 4091–4103, 2005.
- [7] F. Srohrabi and W. Yu, "Hybrid digital and analog beamforming design for large-scale antenna arrays," *IEEE J. Sel. Topics Signal Process.*, vol. 10, no. 3, pp. 501–513, 2016.
- [8] O. El Ayach, S. Rajagopal, S. Abu-Surra, Z. Pi, and R. W. Heath, "Spatially sparse precoding in millimeter wave MIMO systems," *IEEE Trans. Wireless Commun.*, vol. 13, no. 3, pp. 1499–1513, 2014.
- [9] R. J. Mailloux, *Phased array antenna handbook*, 2nd ed. Artech house, 2005.
- [10] —, "Phased array theory and technology," *Proc. IEEE*, vol. 70, no. 3, pp. 246–291, 1982.
- [11] R. Rotman, M. Tur, and L. Yaron, "True time delay in phased arrays," *Proc. IEEE*, vol. 104, no. 3, pp. 504–518, 2016.
- [12] M. Longbrake, "True time-delay beamsteering for radar," in *IEEE Nat. Aerosp. Electron. Conf.*, 2012, pp. 246–249.
- [13] Z. Cao, Q. Ma, A. B. Smolders, Y. Jiao, M. J. Wale, C. W. Oh, H. Wu, and A. M. J. Koonen, "Advanced integration techniques on broadband millimeter-wave beam steering for 5G wireless networks and beyond," *IEEE J. Quantum Electron.*, vol. 52, no. 1, pp. 1–20, 2015.
- [14] M. M. Mojahedian, M. Attarifar, and A. Lozano, "Spatial-wideband effect in line-of-sight MIMO communication," in *IEEE Int'l Conf. Commun.*, 2022, pp. 3972–3977.
- [15] L. Steinweg, C. Carta, and F. Ellinger, "A hybrid true-time and phase-delayed approach for millimeter-wave beam steering," *IEEE Trans. Microwave Theory Techn.*, vol. 70, no. 9, pp. 4318–4327, 2022.
- [16] C.-C. Lin *et al.*, "Wideband beamforming with rainbow beam training using reconfigurable true-time-delay arrays for millimeter-wave wireless," *IEEE Circuits Syst. Mag.*, vol. 22, no. 4, pp. 6–25, 2022.
- [17] X. Liu and D. Qiao, "Space-time block coding-based beamforming for beam squint compensation," *IEEE Wireless Commun. Lett.*, vol. 8, no. 1, pp. 241–244, 2018.
- [18] F. Gao, B. Wang, C. Xing, J. An, and G. Y. Li, "Wideband beamforming for hybrid massive MIMO terahertz communications," *IEEE J. Sel. Areas Commun.*, vol. 39, no. 6, pp. 1725–1740, 2021.
- [19] M. Ma, N. T. Nguyen, and M. Juntti, "Closed-form hybrid beamforming solution for spectral efficiency upper bound maximization in mmWave MIMO-OFDM systems," in *IEEE Veh. Technol. Conf.*, 2021, pp. 1–5.
- [20] N. T. Nguyen, J. Kokkonen, and M. Juntti, "Beam squint effects in THz communications with UPA and ULA: Comparison and hybrid beamforming design," in *IEEE Global Commun. Conf. Workshops*, 2022, pp. 1754–1759.
- [21] A. M. Elbir, "A unified approach for beam-split mitigation in terahertz wideband hybrid beamforming," *IEEE Trans. Veh. Technol.*, vol. 72, no. 9, pp. 12355–12360, 2023.
- [22] M. Cai, K. Gao, D. Nie, B. Hochwald, J. N. Laneman, H. Huang, and K. Liu, "Effect of wideband beam squint on codebook design in phased-array wireless systems," in *IEEE Global Commun. Conf.*, 2016, pp. 1–6.
- [23] M. Cai, J. N. Laneman, and B. Hochwald, "Beamforming codebook compensation for beam squint with channel capacity constraint," in *IEEE Int'l Symp. Inf. Theory*, 2017, pp. 76–80.
- [24] B. Wang, M. Jian, F. Gao, G. Y. Li, and H. Lin, "Beam squint and channel estimation for wideband mmwave massive MIMO-OFDM systems," *IEEE Trans. Signal Process.*, vol. 67, no. 23, pp. 5893–5908, 2019.
- [25] K. Dovelos, M. Matthaiou, H. Q. Ngo, and B. Bellalta, "Channel estimation and hybrid combining for wideband terahertz massive MIMO systems," *IEEE J. Sel. Areas Commun.*, vol. 39, no. 6, pp. 1604–1620, 2021.
- [26] L. Dai, J. Tan, Z. Chen, and H. V. Poor, "Delay-phase precoding for wideband THz massive MIMO," *IEEE Trans. Wireless Commun.*, vol. 21, no. 9, pp. 7271–7286, 2022.
- [27] J. H. Brady and A. M. Sayeed, "Wideband communication with high-dimensional arrays: New results and transceiver architectures," in *IEEE Int'l Conf. Commun. Workshop*, 2015, pp. 1042–1047.
- [28] H.-J. Song and T. Nagatsuma, "Present and future of terahertz communications," *IEEE Trans. Terahertz Sci. Technol.*, vol. 1, no. 1, pp. 256–263, 2011.
- [29] A. Alkhateeb and R. W. Heath, "Frequency selective hybrid precoding for limited feedback millimeter wave systems," *IEEE Trans. Commun.*, vol. 64, no. 5, pp. 1801–1818, 2016.
- [30] R. C. Hansen, *Phased array antennas*. John Wiley & Sons, 2009.
- [31] S. Park, A. Alkhateeb, and R. W. Heath, "Dynamic subarrays for hybrid precoding in wideband mmWave MIMO systems," *IEEE Trans. Wireless Commun.*, vol. 16, no. 5, pp. 2907–2920, 2017.
- [32] H. Do, N. Lee, and A. Lozano, "Line-of-sight MIMO via intelligent reflecting surface," *IEEE Trans. Wireless Commun.*, vol. 22, no. 6, pp. 4215–4231, 2023.
- [33] D. E. Knuth, "Two notes on notation," *The American Mathematical Monthly*, vol. 99, no. 5, pp. 403–422, 1992.
- [34] D. Slepian and H. O. Pollak, "Prolate spheroidal wave functions, Fourier analysis and uncertainty—I," *Bell System Tech. J.*, vol. 40, no. 1, pp. 43–63, 1961.
- [35] M. Dohler, R. W. Heath, A. Lozano, C. B. Papadimas, and R. A. Valenzuela, "Is the PHY layer dead?" *IEEE Commun. Mag.*, vol. 49, no. 4, pp. 159–165, 2011.
- [36] A. Townsend and L. N. Trefethen, "An extension of chebfun to two dimensions," *SIAM J. Scientific Comput.*, vol. 35, no. 6, pp. C495–C518, 2013.
- [37] D. Zhang, Y. Wang, X. Li, and W. Xiang, "Hybridly connected structure for hybrid beamforming in mmwave massive MIMO systems," *IEEE Trans. Commun.*, vol. 66, no. 2, pp. 662–674, 2017.
- [38] H. Do, N. Lee, and A. Lozano, "Parabolic wavefront model for line-of-sight MIMO channels," *IEEE Trans. Wireless Commun.*, 2023.
- [39] S.-H. Park, B. Kim, D. K. Kim, L. Dai, K.-K. Wong, and C.-B. Chae, "Beam squint in ultra-wideband mmWave systems: RF lens array vs. phase-shifter-based array," *IEEE Wireless Commun.*, vol. 30, no. 4, pp. 82–89, 2023.
- [40] B. Zhai, Y. Zhu, A. Tang, and X. Wang, "THzPrism: Frequency-based beam spreading for terahertz communication systems," *IEEE Wireless Commun. Lett.*, vol. 9, no. 6, pp. 897–900, 2020.
- [41] I. K. Jain, R. R. Vennam, R. Subbaraman, and D. Bharadia, "mmFlexible: Flexible directional frequency multiplexing for multi-user mmwave networks," in *IEEE Int'l Conf. Comput. Commun.*, 2023.
- [42] N. J. Myers and R. W. Heath, "InFocus: A spatial coding technique to mitigate misfocus in near-field LoS beamforming," *IEEE Trans. Wireless Commun.*, vol. 21, no. 4, pp. 2193–2209, 2021.
- [43] R. A. Horn and C. R. Johnson, *Matrix analysis*. Cambridge university press, 2012.